

Hybrid Contact Preintegration for Visual-Inertial-Contact State Estimation within Factor Graphs

Ross Hartley, Maani Ghaffari Jadidi, Lu Gan, Jiunn-Kai Huang, Jessie W. Grizzle, and Ryan M. Eustice

Abstract—The factor graph framework is a convenient modeling technique for robotic state estimation and sensor fusion where states are represented as nodes and measurements are modeled as factors. In designing a sensor fusion framework using factor graphs for legged robots, one often has access to visual, inertial, encoders, and contact sensors. While visual-inertial odometry has been studied extensively in this framework, the addition of a preintegrated contact factor for legged robots has been proposed recently. In this work, to cope with the problem of switching contact frames which was not addressed previously, we propose a hybrid contact preintegration that does not require the addition of frequently broken contact factors into the estimation factor graph. This paper presents a novel method for preintegrating contact information through an arbitrary number of contact switches. The proposed hybrid modeling approach reduces the number of required variables in the nonlinear optimization problem by only requiring new states to be added alongside camera or selected keyframes. This method is evaluated using real experimental data collected from a Cassie-series robot where the trajectory of the robot produced by a motion capture system is used as a proxy for ground truth data. The evaluation shows that inclusion of the proposed preintegrated hybrid contact factor alongside visual-inertial navigation systems improves robustness to vision failure as well as the estimation accuracy for legged robots while its generalization makes it more accessible for legged platforms.

I. INTRODUCTION AND RELATED WORK

Long-term state estimation and mapping for legged robots require a flexible sensor fusion framework that allows for reducing the drift and correcting the past estimates as the robot perceives new information. During long-term missions, odometry systems can drift substantially since the absolute position and yaw (rotation about gravity) are unobservable [1], leading to an unbounded growth in the covariance of the estimate and an undesirable expansion of the search space for data association tasks. Factor graph smoothing framework [2]–[5] offers suitable machineries for building such systems in which real-time performance is achieved by exploiting the sparse structure of the Simultaneous Localization and Mapping (SLAM) problem [6], [7]. In addition, the incorporation of loop-closures [7] into the graph, upon availability, is convenient.

Legged robot perception often involves fusing leg odometry, Inertial Measurement Unit (IMU), and visual/depth measurements to infer the robot trajectory, controller inputs such as velocity, and calibration parameters [8]–[11]. The challenge in such perception problems is the rigorous real-time performance requirements in legged robots arising from

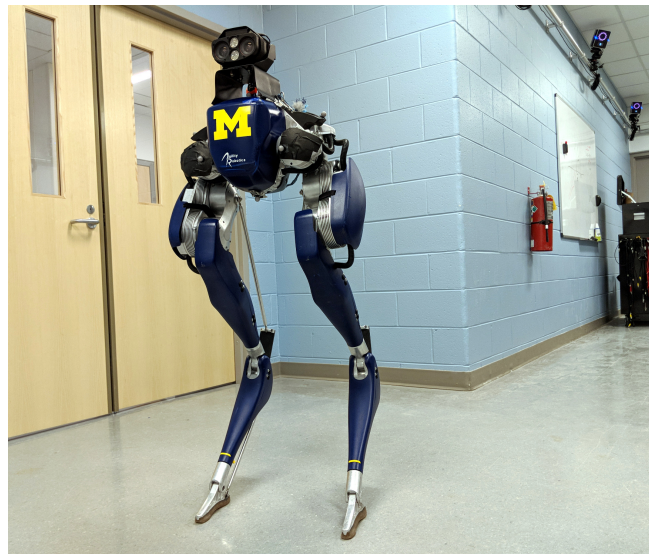


Fig. 1: Experiments were conducted on a Cassie-series robot designed by Agility Robotics in an indoor laboratory environment. The motion capture system is used to record the robot trajectory as a proxy for ground truth data. The Cassie-series robot has 20 degrees of freedom, 10 actuators, joint encoders, an IMU, and mounted with a Multisense S7 stereo camera.

their direct and switching contact with the environment [1], [12]–[15]. Furthermore, leg odometry involves estimating relative transformations and velocity using kinematic and contact information, which can be noisy due to the encoder noise and foot slip [16].

Towards building a perception system for legged robots suitable for long-term state estimation and mapping, in our previous work [17], we developed two novel factors that integrate the use of multi-link Forward Kinematics (FK) and the notion of contact between the robotic system and the environment into the factor graph framework. While the new factors improved the estimator’s performance, new challenges emerged due to frequent switching contacts as the robot navigates through an environment. For example, for a hexapod robot, maintaining and tracking one contact pose per leg leads to an overly complicated implementation. However, the inclusion of the contact frame pose in the state is beneficial as the knowledge of the contact frame and the estimated map provides additional loop-closures.

In this paper, we generalize the idea of the preintegrated contact factor in [17] to a *hybrid preintegration contact factor* that alleviates the effect of the frequently broken contact with an environment. We develop a novel method for preintegrating contact information through an arbitrary number of contact switches. The proposed hybrid modeling

The authors are with the College of Engineering, University of Michigan, Ann Arbor, MI 48109 USA {rosshart, maanigj, ganlu, bjhuang, grizzle, eustice}@umich.edu.

approach reduces the number of required variables in the nonlinear optimization problem by only requiring new states to be added alongside camera or selected keyframes. The present work has the following contributions:

- i. A generic forward kinematic factor modeled in $SE(3)$ using the manipulator Jacobian that supports both prismatic and revolute joints; the factor incorporates noisy encoder measurements to estimate an end-effector pose at any time-step;
- ii. A hybrid preintegrated contact factor modeled in $SE(3)$ that allows for an arbitrary number of contact switches between camera or selected keyframes.
- iii. Real-time implementation and experimental evaluation of the derived factors on a Cassie-series biped robot in an indoor laboratory environment where ground truth data was collected using a motion capture system.

The remainder of this paper is organized as follows. Section II provides the mathematical background and preliminaries. We formulate the problem using the factor graph approach in Section III. Section IV explains the forward kinematic modeling and derives the forward kinematic factor. The proposed hybrid rigid contact model and hybrid contact preintegration are derived in Section V. Experimental evaluations of the proposed methods on a 3D biped robot (shown in Fig. 1) are presented in Section VI. Finally, Section VII concludes the paper and provides future work suggestions.

II. MATHEMATICAL BACKGROUND AND PRELIMINARIES

We first review the Lie group theory corresponding to the rotation and motion groups [18], [19]. Afterwards, we discuss the optimization technique on matrix Lie groups [20] and the choice of retraction for deriving forward kinematic and hybrid preintegrated contact factors.

Matrices are capitalized in bold, such as in \mathbf{X} , and vectors are column-wise in lower case bold type, such as in \mathbf{x} . We denote $\|\mathbf{e}\|_{\Sigma}^2 \triangleq \mathbf{e}^T \Sigma^{-1} \mathbf{e}$. The n -by- n identity matrix and the n -by- m matrix of zeros are denoted by \mathbf{I}_n and $\mathbf{0}_{n,m}$ respectively. The vector constructed by stacking x_i , $\forall i \in \{1, \dots, n\}$ is denoted by $\text{vec}(x_1, \dots, x_n)$. The covariance of a random vector is denoted by $\text{Cov}(\cdot)$. Finally, we denote the base frame of the robot by \mathbf{B} , the world frame by \mathbf{W} , and contact frame by \mathbf{C} .

A. Matrix Lie Group of Rotation and Motion in \mathbb{R}^3

The general linear group of degree n , denoted by $GL_n(\mathbb{R})$, is the set of all $n \times n$ nonsingular real matrices, where the group binary operation is the ordinary matrix multiplication. The three-dimensional (3D) special orthogonal group, denoted by $SO(3) = \{\mathbf{R} \in GL_3(\mathbb{R}) \mid \mathbf{R}\mathbf{R}^T = \mathbf{I}_3, \det \mathbf{R} = +1\}$ is the rotation group on \mathbb{R}^3 . The 3D special Euclidean group, denoted by

$$SE(3) = \{\mathbf{H} = \begin{bmatrix} \mathbf{R} & \mathbf{p} \\ \mathbf{0}_{1 \times 3} & 1 \end{bmatrix} \in GL_4(\mathbb{R}) \mid \mathbf{R} \in SO(3), \mathbf{p} \in \mathbb{R}^3\}$$

is the group of rigid transformations on \mathbb{R}^3 . The Lie algebra (tangent space at the identity together with Lie bracket) of

$SO(3)$, denoted by $\mathfrak{so}(3)$, is the set of 3×3 skew-symmetric matrices such that for any $\boldsymbol{\omega} \triangleq \text{vec}(\omega_1, \omega_2, \omega_3) \in \mathbb{R}^3$:

$$\boldsymbol{\omega}^\wedge \triangleq \begin{bmatrix} 0 & -\omega_3 & \omega_2 \\ \omega_3 & 0 & -\omega_1 \\ -\omega_2 & \omega_1 & 0 \end{bmatrix}$$

and $(\boldsymbol{\omega}^\wedge)^\vee = \boldsymbol{\omega}$. The Lie algebra of $SE(3)$, denoted by $\mathfrak{se}(3)$, can be identified by 4×4 matrices such that for any $\boldsymbol{\omega}, \mathbf{v} \in \mathbb{R}^3$ and the twist is defined as $\boldsymbol{\xi} \triangleq \text{vec}(\boldsymbol{\omega}, \mathbf{v}) \in \mathbb{R}^6$:

$$\boldsymbol{\xi}^\wedge \triangleq \begin{bmatrix} \boldsymbol{\omega}^\wedge & \mathbf{v} \\ \mathbf{0}_{1 \times 3} & 0 \end{bmatrix} \quad (1)$$

where the wedge operator ($^\wedge$) for twist is overloaded.

The exponential map $\exp : \mathfrak{se}(3) \rightarrow SE(3)$ can be used to map a member of $\mathfrak{se}(3)$ around a neighborhood of zero to a member of $SE(3)$ around a neighborhood of the identity. The logarithm map is the inverse, i.e., $\log : SE(3) \rightarrow \mathfrak{se}(3)$, and $\exp(\log(\mathbf{H})) = \mathbf{H}$, $\mathbf{H} \in SE(3)$. Now we can define the difference between a transformation $\mathbf{H} \in SE(3)$ and its estimate with a small perturbation $\tilde{\mathbf{H}} \in SE(3)$ as [19], [21]:

$$\boldsymbol{\epsilon}^\wedge = \log(\mathbf{H}^{-1} \tilde{\mathbf{H}})$$

where $\boldsymbol{\epsilon}^\wedge \in \mathfrak{se}(3)$. To define the norm and covariance of the error term, we exploit the fact that $\mathfrak{se}(3)$ is isomorphic to \mathbb{R}^6 , i.e., $\boldsymbol{\epsilon}^\wedge \mapsto \boldsymbol{\epsilon} \in \mathbb{R}^6$ using the $^\vee$ operator. Therefore, we can define the 6×6 covariance matrix conveniently as $\Sigma_\boldsymbol{\epsilon} = \text{Cov}[\boldsymbol{\epsilon}]$. We use the following adopted simplified notations from [5]:

$$\begin{aligned} \text{Exp} : \mathbb{R}^6 &\ni \boldsymbol{\xi} &\rightarrow \exp(\boldsymbol{\xi}^\wedge) &\in SE(3) \\ \text{Log} : SE(3) &\ni \mathbf{H} &\rightarrow \log(\mathbf{H})^\vee &\in \mathbb{R}^6. \end{aligned}$$

The adjoint representation of a Lie group is a linear map that captures the non-commutative structure of the group. For $SE(3)$, the matrix representation of the adjoint map is given by:

$$\text{Ad}_{\mathbf{H}} = \begin{bmatrix} \mathbf{R} & \mathbf{0}_{3 \times 3} \\ \mathbf{p}^\wedge \mathbf{R} & \mathbf{R} \end{bmatrix} \quad (2)$$

For any $\mathbf{H} \in SE(3)$ and $\boldsymbol{\xi} \in \mathfrak{se}(3)$, the adjoint map asserts [19].

$$\text{Ad}_{\mathbf{H}} \boldsymbol{\xi}^\wedge = \mathbf{H} \boldsymbol{\xi}^\wedge \mathbf{H}^{-1} \Rightarrow \text{Exp}(\text{Ad}_{\mathbf{H}} \boldsymbol{\xi}) = \mathbf{H} \text{Exp}(\boldsymbol{\xi}) \mathbf{H}^{-1}$$

B. Retraction Map and Optimization on Manifold

Given a retraction mapping and the associated manifold, we can optimize over the manifold by iteratively *lifting* the cost function of our optimization problem to the tangent space, solving the reparameterized problem, and then mapping the updated solution back to the manifold using the retraction [20]. For $SE(3)$ we use its exponential map as the natural retraction, $\mathcal{R}_{\mathbf{H}}(\delta \boldsymbol{\xi}) = \mathbf{H} \text{Exp}(\delta \boldsymbol{\xi})$, where $\delta \boldsymbol{\xi} \in \mathbb{R}^6$ is the twist defined earlier in (1). Therefore, lifting involves the following retraction on the base and the contact poses:

$$\mathbf{X}_i \leftarrow \mathbf{X}_i \text{Exp}(\delta \mathbf{x}_i) \quad \mathbf{C}_i \leftarrow \mathbf{C}_i \text{Exp}(\delta \mathbf{c}_i) \quad (3)$$

allowing the Jacobians of the residuals easy to compute. The Jacobians for the forward kinematic factors are derived in the following sections.

III. PROBLEM STATEMENT AND FORMULATION

In the following, we formulate the state estimation problem using the factor graph framework where independent measurements can be incorporated by introducing additional factors based on the associated measurement models. The biped robot is equipped with a stereo camera, an IMU mounted on the torso, joint encoders, and binary contact sensors on the feet. Without loss of generality, we assume the IMU and camera are collocated with the base frame of the robot.

A. State Representation

The state variables (at time t_i) include the body 3D pose, $\mathbf{H}_{\text{WB}}(t) \in \text{SE}(3)$, and velocity, ${}_{\text{w}}\mathbf{v}_{\text{WB}}(t) \in \mathbb{R}^3$, in the world frame, the rigid contact 3D pose in the world frame, $\mathbf{H}_{\text{WC}}(t) \in \text{SE}(3)$, and the IMU bias, $\mathbf{b}(t) \triangleq \text{vec}(\mathbf{b}^a(t), \mathbf{b}^g(t)) \in \mathbb{R}^6$, where $\mathbf{b}^a(t) \in \mathbb{R}^3$ and $\mathbf{b}^g(t) \in \mathbb{R}^3$ are the accelerometer and gyroscope biases, respectively. All together, the state at any time-step i is a tuple as follows:

$$\mathcal{T}_i \triangleq (\mathbf{H}_{\text{WB}}(t), {}_{\text{w}}\mathbf{v}_{\text{WB}}(t), \mathbf{H}_{\text{WC}}(t), \mathbf{b}(t)) \triangleq (\mathbf{X}_i, \mathbf{v}_i, \mathbf{C}_i, \mathbf{b}_i) \quad (4)$$

Further, it is convenient to denote the trajectory of the state variables up to time-step k by $\mathcal{X}_k \triangleq \bigcup_{i=1}^k \mathcal{T}_i$. Foot slip is the major source of drift in leg odometry. The inclusion of the contact pose in the state tuple allows for isolating the noise at the contact point.

B. Factor Graph Formulation

Let $\mathcal{L}_{ij} \in \text{SE}(3)$ be a perceptual loop-closure measurement relating poses at time-steps i and j ($j > i$) computed from an independent sensor, e.g. using a point cloud matching algorithm. The forward kinematic measurements at time-step i are denoted by \mathcal{F}_i . The IMU and contact sensors provide measurements at higher frequencies. Between any two time-steps i and j , we denote the set of all IMU and contact measurements by \mathcal{I}_{ij} and \mathcal{C}_{ij} , respectively. Let \mathcal{K}_k be the index set of time-steps (or key-frames) up to time-step k . We denote the set of all measurements up to time-step k by $\mathcal{Z}_k \triangleq \{\mathcal{L}_{ij}, \mathcal{I}_{ij}, \mathcal{F}_i, \mathcal{C}_{ij}\}_{i,j \in \mathcal{K}_k}$.

By assuming the measurements are conditionally independent and are corrupted by additive zero mean white Gaussian noise, the posterior probability of the *full SLAM* problem can be written as $p(\mathcal{X}_k | \mathcal{Z}_k) \propto p(\mathcal{X}_0) p(\mathcal{Z}_k | \mathcal{X}_k)$, where

$$p(\mathcal{Z}_k | \mathcal{X}_k) = \prod_{i,j \in \mathcal{K}_k} p(\mathcal{L}_{ij} | \mathcal{X}_j) p(\mathcal{I}_{ij} | \mathcal{X}_j) p(\mathcal{F}_i | \mathcal{X}_i) p(\mathcal{C}_{ij} | \mathcal{X}_j).$$

The *Maximum-A-Posteriori* (MAP) estimate of \mathcal{X}_k can be computed by solving the following optimization problem:

$$\underset{\mathcal{X}_k}{\text{minimize}} \quad -\log p(\mathcal{X}_k | \mathcal{Z}_k)$$

in which due to the noise assumption mentioned earlier is equivalent to the following nonlinear least-squares problem:

$$\underset{\mathcal{X}_k}{\text{minimize}} \quad \|\mathbf{r}_0\|_{\Sigma_0}^2 + \sum_{i,j \in \mathcal{K}_k} \|\mathbf{r}_{\mathcal{L}_{ij}}\|_{\Sigma_{\mathcal{L}_{ij}}}^2 + \sum_{i,j \in \mathcal{K}_k} \|\mathbf{r}_{\mathcal{I}_{ij}}\|_{\Sigma_{\mathcal{I}_{ij}}}^2 \\ + \sum_{i \in \mathcal{K}_k} \|\mathbf{r}_{\mathcal{F}_i}\|_{\Sigma_{\mathcal{F}_i}}^2 + \sum_{i,j \in \mathcal{K}_k} \|\mathbf{r}_{\mathcal{C}_{ij}}\|_{\Sigma_{\mathcal{C}_{ij}}}^2$$

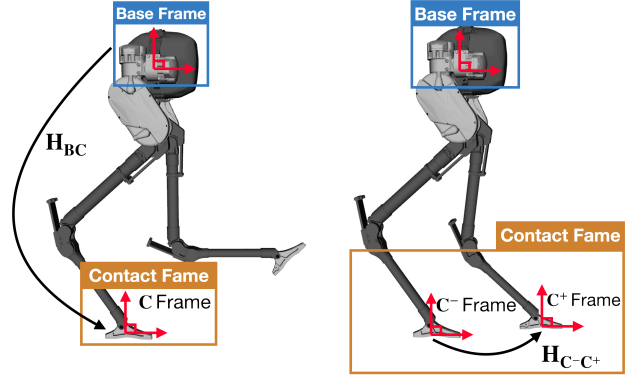


Fig. 2: In this paper, we refer to two separate forward kinematics functions. The pose of the current contact frame relative to the base frame is denoted by \mathbf{H}_{BC} . When the robot has multiple points of contact with the environment, it is possible to transfer this contact from from one frame to another. This transfer of contact is captured by the homogeneous transform $\mathbf{H}_{\text{C-C}^+}$.

where \mathbf{r}_0 and Σ_0 represents the prior over the initial state and serves to anchor the graph, $\mathbf{r}_{\mathcal{L}_{ij}}$, $\mathbf{r}_{\mathcal{I}_{ij}}$, $\mathbf{r}_{\mathcal{F}_i}$, $\mathbf{r}_{\mathcal{C}_{ij}}$ are the residual terms associated with the loop closure, IMU, forward kinematic, and contact measurements respectively, i.e. the error between the measured and predicted values given the state, and $\Sigma_{\mathcal{L}_{ij}}$, $\Sigma_{\mathcal{I}_{ij}}$, $\Sigma_{\mathcal{F}_i}$, $\Sigma_{\mathcal{C}_{ij}}$ are the corresponding covariance matrices.

IV. FORWARD KINEMATICS

Forward kinematics refers to the process of computing the relative pose transformation between two frames of a multi-link system. Each individual joint displacement describes how the child link moves with respect to the parent one. This joint displacement can either be an angle (revolute joints) or a distance (prismatic joints).

Let $\alpha \in \mathbb{R}^N$ denote the vector of joint displacements for a general robot. Without loss of generality, we define a *base frame* on the robot, denoted B , that is assumed to be collocated with both the IMU and the camera frames. When the robot is in contact with the static environment, we can also define a *contact frame*, denoted C , on the robot at the point of contact. The homogeneous transformation between the base frame and the contact frame is defined by:

$$\mathbf{H}_{\text{BC}}(\alpha) \triangleq \begin{bmatrix} \mathbf{R}_{\text{BC}}(\alpha) & \text{Bp}_{\text{BC}}(\alpha) \\ \mathbf{0}_{1 \times 3} & 1 \end{bmatrix} \quad (5)$$

where $\mathbf{R}_{\text{BC}}(\alpha)$ and $\text{Bp}_{\text{BC}}(\alpha)$ denote the relative orientation and position of the contact frame with respect to the base frame.

When there are two points in contact with the static environment, it is possible to “transfer” the contact frame from one point to the other (shown in Figure 2). Let C^- denote the old contact frame and C^+ denote the new contact frame. Then, the homogeneous transformation between the old frame and the new frame is defined by:

$$\mathbf{H}_{\text{C}^-\text{C}^+}(\alpha) \triangleq \begin{bmatrix} \mathbf{R}_{\text{C}^-\text{C}^+}(\alpha) & \text{Cp}_{\text{C}^-\text{C}^+}(\alpha) \\ \mathbf{0}_{1 \times 3} & 1 \end{bmatrix} \quad (6)$$

where $\mathbf{R}_{\text{C}^-\text{C}^+}(\alpha)$ and $\text{Cp}_{\text{C}^-\text{C}^+}(\alpha)$ denote the relative orientation and position of the new contact frame with respect to the old contact frame.

A. Measurements

We assume that every joint on the robot is equipped with a set of joint encoders that can measure the joint displacement. These encoder measurements, $\tilde{\alpha}$, are assumed to be corrupted with Gaussian white noise. This is an explicit measurement coming from physical sensors located on the robot.

$$\tilde{\alpha}(t) = \alpha(t) + \eta^\alpha(t) \quad \eta^\alpha(t) \sim \mathcal{N}(\mathbf{0}_{N \times 1}, \Sigma^\alpha(t)) \quad (7)$$

The geometric (or manipulator) Jacobian, denoted $\mathbf{J}(\alpha)$, provides a method for computing the angular and linear velocity of an end-effector given the vector of joint velocities [18]. In a similar manner, we can use the Jacobian to map incremental angles to changes in the end-effector pose. Let $\mathbf{J}_{\text{BC}}(\alpha)$ denote the body manipulator Jacobian of the forward kinematics function (5). Then, the following relationship holds:

$$c\xi_{\text{WC}} \delta t = \mathbf{J}_{\text{BC}}(\alpha) \delta \alpha \quad (8)$$

where $\delta \alpha$ and δt are incremental encoder and time quantities and $c\xi_{\text{WC}}$ denotes the vector of angular and linear velocities of the contact frame due to $\delta \alpha$ (measured in the contact frame). We perform Euler integration using (8) to provide a method for factoring out the noise from the forward kinematics equations. Up to a first order approximation, (5) can be factored as:

$$\mathbf{H}_{\text{BC}}(\tilde{\alpha}(t) - \eta^\alpha(t)) \approx \mathbf{H}_{\text{BC}}(\tilde{\alpha}(t)) \text{Exp}(-\mathbf{J}_{\text{BC}}(\tilde{\alpha}(t))\eta^\alpha(t)) \quad (9)$$

A similar approximation can be found for (6), albeit with a different Jacobian.

$$\mathbf{H}_{\text{C}^*}(\tilde{\alpha}(t) - \eta^\alpha(t)) \approx \mathbf{H}_{\text{C}^*}(\tilde{\alpha}(t)) \text{Exp}(-\mathbf{J}_{\text{C}^*}(\tilde{\alpha}(t))\eta^\alpha(t)) \quad (10)$$

Remark 1. *In general, the manipulator Jacobian can be derived as spatial or body manipulator Jacobian [18], and based on this choice, the noise can appear on the left or right side of the rotation/rigid body transformation, respectively.*

B. Forward Kinematic Factor

The goal of this section is to derive a general *forward kinematic factor* that can be used in the factor graph framework. This will be a unary factor that relates two poses through the forward kinematics equations while accounting for encoder noise. We derive it here for relating the base and contact frames.

The orientation and position of the contact frame with respect to the world frame are given by:

$$\mathbf{H}_{\text{WC}}(t) = \mathbf{H}_{\text{WB}}(t) \mathbf{H}_{\text{BC}}(\alpha(t)) \quad (11)$$

Substituting in the state variables at time t_i (4), the forward kinematic equations (5) yields:

$$\mathbf{C}_i = \mathbf{X}_i \mathbf{H}_{\text{BC}}(\tilde{\alpha}_i - \eta_i^\alpha) \quad (12)$$

We can now use the first order approximation (9) to factor

out the encoder noise to give the following expressions:

$$\mathbf{C}_i = \mathbf{X}_i \mathbf{H}_{\text{BC}}(\tilde{\alpha}_i) \text{Exp}(-\mathbf{J}_{\text{BC}}(\tilde{\alpha}_i)\eta_i^\alpha) \quad (13)$$

Defining the zero-mean white Gaussian forward kinematic noise terms, $\delta \mathbf{c}_i \triangleq \mathbf{J}_{\text{BC}}(\tilde{\alpha}_i)\eta_i^\alpha$ allows us to write out the *forward kinematics measurement model*:

$$\mathbf{H}_{\text{BC}}(\tilde{\alpha}_i) = \mathbf{X}_i^\top \mathbf{C}_i \text{Exp}(\delta \mathbf{c}_i) \quad (14)$$

where the forward kinematics noise is characterized by $\delta \mathbf{c}_i \sim \mathcal{N}(\mathbf{0}_{6 \times 1}, \Sigma_{\mathcal{F}_i})$. The residual errors are defined in the tangent space and can be written as:

$$\mathbf{r}_{\mathcal{F}_i} = \text{Log}\left(\mathbf{C}_i^\top \mathbf{X}_i \mathbf{H}_{\text{BC}}(\tilde{\alpha}_i)\right) \quad (15)$$

The covariance is computed through the following linear transformation:

$$\Sigma_{\mathcal{F}_i} = \mathbf{J}_{\text{BC}}(\tilde{\alpha}_i) \Sigma_i^\alpha \mathbf{J}_{\text{BC}}^\top(\tilde{\alpha}_i) \quad (16)$$

where $\mathbf{J}(\tilde{\alpha}_i)$ is the body manipulator Jacobian evaluated at the current encoder measurements and Σ_i^α denotes the encoder covariance matrix at time t_i .

V. HYBRID CONTACT PREINTEGRATION

A continuous hybrid dynamical system, \mathcal{H} , can be defined with a continuous dynamics function, $f(\cdot)$, a discrete transition map, $\Delta(\cdot)$, and a switching surface, \mathcal{S} [22]. Trajectories of the hybrid dynamical system evolve according to the continuous dynamics, until the switching surface it hit. At those moments, the state gets mapped through the discrete transition map, after which the trajectory continues according to the continuous dynamics again. The general form of this system can be expressed as follows.

$$\mathcal{H} : \begin{cases} \dot{x}(t) = f(x, t) & (x^-, t^-) \notin \mathcal{S} \\ x^+ = \Delta(x^-) & (x^-, t^-) \in \mathcal{S} \end{cases} \quad (17)$$

As long as the number of contact points is greater than or equal to one, the switching contact frame dynamics can be modeled as a hybrid system:

$$\mathcal{H} : \begin{cases} \dot{\mathbf{H}}_{\text{WC}}(t) = \mathbf{H}_{\text{WC}}(t) (c\xi_{\text{WC}}(t))^\wedge & t^- \notin \mathcal{S} \\ \mathbf{H}_{\text{WC}^*} = \mathbf{H}_{\text{WC}} \mathbf{H}_{\text{C}^*} & t^- \in \mathcal{S} \end{cases} \quad (18)$$

with the switching surface, \mathcal{S} is simply modeled as the set of all times where contact is switched from one frame to another. Since the sensor measurements are coming in at discrete time-steps, we perform Euler integration from time t to $t + \Delta t$ to discretize the continuous hybrid contact dynamics (18), forming the following discrete hybrid system:

$$\mathcal{H} : \begin{cases} \mathbf{H}_{\text{WC}}(t + \Delta t) = \mathbf{H}_{\text{WC}}(t) \text{Exp}(c\xi_{\text{WC}}(t)\Delta t) & t^- \notin \mathcal{S} \\ \mathbf{H}_{\text{WC}^*} = \mathbf{H}_{\text{WC}} \mathbf{H}_{\text{C}^*} & t^- \in \mathcal{S} \end{cases} \quad (19)$$

Physically, the continuous dynamics function, f , describes how a single contact frame moves over time while contact is maintained. When a new contact frame is detected, the new contact pose can be computed by applying the transition

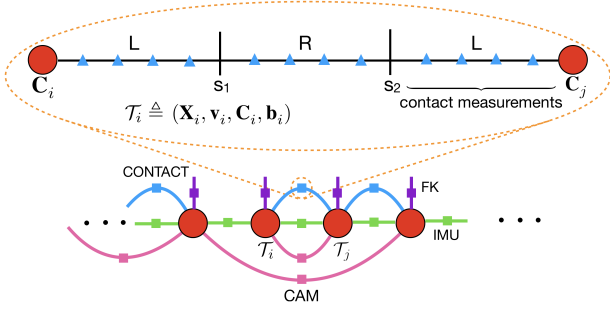


Fig. 3: In the factor graph framework, we are estimating the robot’s state along a discretized trajectory (denoted by red circles). Each independent sensor measurement can provide a “factor” (denoted by lines) that constrains the state at separate time-steps. The proposed hybrid contact factor (shown on top) allows preintegration of high-frequency contact data through an arbitrary number of contact switches. In this example, there are two contact switches, where the robot moves from left-stance (L) to right-stance (R), then back to left stance.

map, $\Delta(\cdot)$, which describes the homogeneous transformation between the old and new contact frames.

A. Measurements

The angular and linear velocity of the contact point is an implicit measurement that is *inferred* through a binary contact sensor: specifically, when this sensor indicates contact, the position of the contact point is *assumed to remain fixed in the world frame*, i.e. the measured velocity is zero. In order to accommodate potential contact slip, the measured velocity is assumed to be corrupted with white Gaussian noise, namely

$$c\tilde{\xi}_{\text{WC}}(t) = \mathbf{0}_{6 \times 1} = c\xi_{\text{WC}}(t) + \boldsymbol{\eta}(t), \quad \boldsymbol{\eta}(t) \sim \mathcal{N}(\mathbf{0}_{6 \times 1}, \boldsymbol{\Sigma}^{\boldsymbol{\eta}}(t)).$$

Using the state variables (4), forward kinematics definition (6), encoder measurements (7), and contact measurements, the hybrid contact dynamics (19) can be written as:

$$\mathcal{H} : \begin{cases} \mathbf{C}_{k+1} = \mathbf{C}_k \text{Exp}(-\boldsymbol{\eta}_k^d \Delta t) & t_k^- \notin \mathcal{S} \\ \mathbf{C}^+ = \mathbf{C}^- \mathbf{H}_{\text{C}^+}(\tilde{\boldsymbol{\alpha}}_k - \boldsymbol{\eta}_k^\alpha) & t_k^- \in \mathcal{S} \end{cases} \quad (20)$$

where $\boldsymbol{\eta}_k^d$, the discrete time contact noise, is computed using the sample time, $\text{Cov}(\boldsymbol{\eta}^d(t)) = \frac{1}{\Delta t} \text{Cov}(\boldsymbol{\eta}(t))$.

Remark 2. $\mathbf{H}_{\text{C}^+}(\boldsymbol{\alpha}_k)$ will depend on the specific contact frames, C^- and C^+ , at time t_k . For example, the forward kinematics function to switch from left foot contact to a right foot contact will be different than the one used to switch from right foot to left foot.

B. Preintegrating Contact Pose

The goal of this section is to formulate a general *hybrid preintegrated contact factor* which relates the contact pose at t_i to the contact pose at t_j . The hybrid nature of this factor comes from the potential switching of contact that occurs naturally in legged locomotion. We preintegrate the high-frequency contact measurements to prevent unnecessary computation allowing efficient implementation of the factor.

Let \mathcal{S} denote the sequence of all time indices associated with contact switches, so that each $s_i \in \mathcal{S}$ represents a single time index where a contact switch occurs. To integrate the hybrid contact dynamics model (20) through these contact

switches, we integrate the up to the next contact switch time t_{s_i} , apply the transition map $\Delta(\cdot)$, and continue the integration. For the following derivations, a concrete example (depicted in Figure 3) is used to make the derivation easier to follow. We later extend the derivation to an arbitrary number of contact switches. For the example shown in Figure 3, there are two contact switches between times t_i and t_j , i.e., $|\mathcal{S}| = 2$. Integrating the discrete hybrid contact model (20) from t_i to t_j yields:

$$\mathbf{C}_j = \mathbf{C}_i \left(\prod_{k=i}^{s_1-1} \text{Exp}(-\boldsymbol{\eta}_k^d \Delta t) \right) \mathbf{H}_{\text{C}^+}(\tilde{\boldsymbol{\alpha}}_{s_1} - \boldsymbol{\eta}_{s_1}^\alpha) \left(\prod_{k=s_1}^{s_2-1} \text{Exp}(-\boldsymbol{\eta}_k^d \Delta t) \right) \mathbf{H}_{\text{C}^+}(\tilde{\boldsymbol{\alpha}}_{s_2} - \boldsymbol{\eta}_{s_2}^\alpha) \left(\prod_{k=s_2}^{j-1} \text{Exp}(-\boldsymbol{\eta}_k^d \Delta t) \right)$$

All noise terms can be shifted to the right by using (10) to factor the noise from the forward kinematics term and the adjoint relation (2) to shift the measured kinematics to the left.

$$\begin{aligned} \mathbf{C}_j &= \mathbf{C}_i \mathbf{H}_{\text{C}^+}(\tilde{\boldsymbol{\alpha}}_{s_1}) \mathbf{H}_{\text{C}^+}(\tilde{\boldsymbol{\alpha}}_{s_2}) \\ &\quad \left(\prod_{k=i}^{s_1-1} \text{Exp}(-\text{Ad}_{\mathbf{H}_{\text{C}^+}^{-1}(\tilde{\boldsymbol{\alpha}}_{s_2})} \text{Ad}_{\mathbf{H}_{\text{C}^+}^{-1}(\tilde{\boldsymbol{\alpha}}_{s_1})} \boldsymbol{\eta}_k^d \Delta t) \right) \\ &\quad \text{Exp}(-\text{Ad}_{\mathbf{H}_{\text{C}^+}^{-1}(\tilde{\boldsymbol{\alpha}}_{s_2})} \mathbf{J}_{\text{C}^+}(\tilde{\boldsymbol{\alpha}}_{s_1}) \boldsymbol{\eta}_{s_1}^\alpha) \\ &\quad \left(\prod_{k=s_1}^{s_2-1} \text{Exp}(-\text{Ad}_{\mathbf{H}_{\text{C}^+}^{-1}(\tilde{\boldsymbol{\alpha}}_{s_2})} \boldsymbol{\eta}_k^d \Delta t) \right) \\ &\quad \text{Exp}(-\mathbf{J}_{\text{C}^+}(\tilde{\boldsymbol{\alpha}}_{s_2}) \boldsymbol{\eta}_{s_2}^\alpha) \left(\prod_{k=s_2}^{j-1} \text{Exp}(-\boldsymbol{\eta}_k^d \Delta t) \right) \end{aligned} \quad (21)$$

After multiplying both sides by \mathbf{C}_i^\top , we arrive at a relative contact pose expression that is independent of states \mathcal{T}_i and \mathcal{T}_j .

$$\Delta \mathbf{C}_{ij} \triangleq \mathbf{C}_i^\top \mathbf{C}_j = \Delta \tilde{\mathbf{C}}_{ij} \text{Exp}(-\delta \mathbf{c}_{ij}) \quad (22)$$

where $\Delta \tilde{\mathbf{C}}_{ij} \triangleq \prod_{n=1}^{|\mathcal{S}|} \mathbf{H}_{\text{C}^+}(\tilde{\boldsymbol{\alpha}}_{s_n})$ represents the *hybrid preintegrated contact measurement*, and $\text{Exp}(-\delta \mathbf{c}_{ij})$ groups all of the noise terms together. This noise term is a product of multiple small rigid body transformations, and therefore can be approximated as a summation in the tangent space using the results from Lemma 1 in the supplementary material [23].

$$\begin{aligned} \delta \mathbf{c}_{ij} &\approx \sum_{k=i}^{s_1-1} \text{Ad}_{\mathbf{H}_{\text{C}^+}^{-1}(\tilde{\boldsymbol{\alpha}}_{s_2})} \text{Ad}_{\mathbf{H}_{\text{C}^+}^{-1}(\tilde{\boldsymbol{\alpha}}_{s_1})} \boldsymbol{\eta}_k^d \Delta t \\ &\quad + \text{Ad}_{\mathbf{H}_{\text{C}^+}^{-1}(\tilde{\boldsymbol{\alpha}}_{s_2})} \mathbf{J}_{\text{C}^+}(\tilde{\boldsymbol{\alpha}}_{s_1}) \boldsymbol{\eta}_{s_1}^\alpha + \sum_{k=s_1}^{s_2-1} \text{Ad}_{\mathbf{H}_{\text{C}^+}^{-1}(\tilde{\boldsymbol{\alpha}}_{s_2})} \boldsymbol{\eta}_k^d \Delta t \\ &\quad + \mathbf{J}_{\text{C}^+}(\tilde{\boldsymbol{\alpha}}_{s_2}) \boldsymbol{\eta}_{s_2}^\alpha + \sum_{k=s_2}^{j-1} \boldsymbol{\eta}_k^d \Delta t \end{aligned}$$

The *hybrid preintegrated contact noise*, $\delta \mathbf{c}_{ij}$, is a summation of zero-mean Gaussian terms, and is therefore also zero-mean and Gaussian. It is possible to generalize this noise expression to an arbitrary number of contact switches, however, it becomes much simpler to do so when looking at the iterative propagation form in the following section.

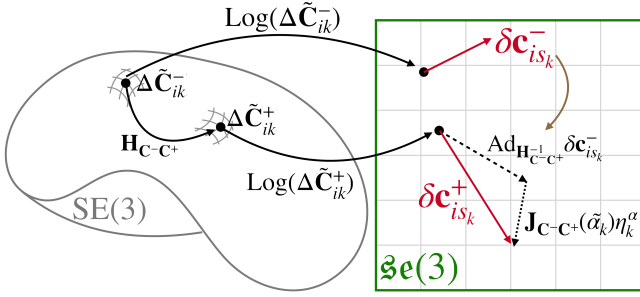


Fig. 4: When a contact switch occurs, the relative contact pose, $\Delta\tilde{\mathbf{C}}_{ik}^-$, gets mapped from one point in $\text{SE}(3)$ to another point, $\Delta\tilde{\mathbf{C}}_{ik}^+$, on the manifold. The contact noise, $\delta\mathbf{c}_{ik}^-$, is represented in the tangent space, $\mathfrak{se}(3)$, and is mapped from the tangent space of $\Delta\tilde{\mathbf{C}}_{ik}^-$ to the tangent space of $\Delta\tilde{\mathbf{C}}_{ik}^+$ through the use of the adjoint map of the forward kinematics transformation, \mathbf{H}_{C-C^+} . However, due to noisy encoders, an additional noise term (computed using the manipulator Jacobian) has to be added to compute $\delta\mathbf{c}_{ik}^+$.

C. Iterative Propagation

It is possible to write both the preintegrated contact measurements, $\Delta\tilde{\mathbf{C}}_{ij}$, and the preintegrated contact noise, $\delta\mathbf{c}_{ij}$, in iterative update forms. This allows the terms to be updated as contact and encoder measurements are coming in. In addition, this form simplifies the expressions and allows for the covariance to be conveniently computed. The following proposition generalizes the hybrid preintegrated contact pose and noise iterative propagation to an arbitrary number of contact switches. The proof is given in the supplementary material.

Proposition 1 (Iterative Propagation of Hybrid Contact Process [23]). *Between any two time-steps t_i and t_j such that $j > i$, starting with $\Delta\tilde{\mathbf{C}}_{ii} = \mathbf{I}_4$, the hybrid preintegrated contact measurement and noise for an arbitrary number of contact switches can be computed using the following hybrid systems:*

$$\tilde{\mathcal{H}} : \begin{cases} \Delta\tilde{\mathbf{C}}_{ik+1} = \Delta\tilde{\mathbf{C}}_{ik} & t_k^- \notin \mathcal{S} \\ \Delta\tilde{\mathbf{C}}_{ik}^+ = \Delta\tilde{\mathbf{C}}_{ik}^- \mathbf{H}_{C-C^+}(\tilde{\alpha}_k) & t_k^- \in \mathcal{S} \end{cases} \quad (23)$$

$$\delta\mathcal{H} : \begin{cases} \delta\mathbf{c}_{ik+1} = \delta\mathbf{c}_{ik} + \boldsymbol{\eta}_k^d \Delta t & t_k^- \notin \mathcal{S} \\ \delta\mathbf{c}_{ik}^+ = \text{Ad}_{\mathbf{H}_{C-C^+}^{-1}(\tilde{\alpha}_k)} \delta\mathbf{c}_{ik}^- + \mathbf{J}_{C-C^+}(\tilde{\alpha}_k) \boldsymbol{\eta}_k^\alpha & t_k^- \in \mathcal{S} \end{cases} \quad (24)$$

An abstract representation of these hybrid systems is shown in Figure 4.

D. Rigid Contact Factor

The relative contact pose expression (22) can be used to define the *preintegrated contact measurement model*:

$$\Delta\tilde{\mathbf{C}}_{ij} = \mathbf{C}_i^\top \mathbf{C}_j \text{Exp}(\delta\mathbf{c}_{ij}) \quad (25)$$

where the zero-mean Gaussian preintegrated contact noise is characterized by $\delta\mathbf{c}_{ij} \sim \mathcal{N}(\mathbf{0}_{6 \times 1}, \boldsymbol{\Sigma}_{C_{ij}})$. In the factor graph framework, the preintegrated contact model represents a binary factor that relates the contact frame pose over consecutive time steps. The residual error is defined in the

tangent space, and can be written as:

$$\mathbf{r}_{C_{ij}} = \text{Log}(\mathbf{C}_j^\top \mathbf{C}_i \Delta\tilde{\mathbf{C}}_{ij}(\tilde{\alpha}_i)) \quad (26)$$

The covariance is computed using the hybrid contact noise model (24), starting with $\boldsymbol{\Sigma}_{C_{ii}} = \mathbf{0}_{6 \times 6}$:

$$\begin{cases} \boldsymbol{\Sigma}_{C_{ik+1}} = \boldsymbol{\Sigma}_{C_{ik}} + \boldsymbol{\Sigma}_k^\eta \Delta t \\ \boldsymbol{\Sigma}_{ik}^+ = \text{Ad}_{\mathbf{H}_{C-C^+}^{-1}(\tilde{\alpha}_k)} \boldsymbol{\Sigma}_{C_{ik}}^- \text{Ad}_{\mathbf{H}_{C-C^+}^{-1}(\tilde{\alpha}_k)}^\top \\ \quad + \mathbf{J}_{C-C^+}(\tilde{\alpha}_k) \boldsymbol{\Sigma}_k^\alpha \mathbf{J}_{C-C^+}^\top(\tilde{\alpha}_k) \end{cases} \quad (27)$$

VI. EXPERIMENTAL RESULTS

We now present experimental evaluations of the proposed factors. In the first experiment, we compare three odometry systems composed by Visual-Inertial-Contact (VIC), Inertial-Contact (IC), and Visual-Inertial (VI) factors. Since the proposed FK model is a unary factor, whenever the contact factor is used, it is assumed that FK factor is also available; therefore, it is not explicitly mentioned for brevity. In the second experiment, we study the effect of losing visual data for a period to see how the contact factor can constrain the graph in the absence of a reliable vision system. In the third experiment, we will evaluate a novel notion called *terrain factor*, where loop-closures can be added to the graph through contact frame poses.

A. Experimental Setup

All experiments are done on a Cassie-series robot designed by Agility Robotics, which has 20 degrees of freedom, 10 actuators, joint encoders, an IMU, along with a Multisense S7 stereo camera mounted on the top of the Cassie robot, containing another IMU, as shown in Fig. 1. Cassie also has four springs (two on each leg) that can be used as a binary contact sensor by thresholding the spring deflection measurements. The Cassie robot has two computers: a MATLAB Simulink Real-Time and a Linux-based system computer. We use the Robot Operating System (ROS) [24] with the User Datagram Protocol (UDP) to communicate sensor data between the two computers. We also integrate the time synchronization algorithm in [25] into our system to ensure all sensory data are synchronized.

The motion capture system developed by Vicon is used as a proxy for ground truth trajectories. The setup consists of 17 motion capture cameras where four markers are attached to Cassie robot to represent its pelvis as well as two markers to represent the orientation of the IMU on Cassie where the base frame of FK is located. The dataset contains the stereo images (20 Hz) and IMU data (750 Hz) from the Multisense S7 camera as well as the joint encoders and IMU data from the Cassie robot (at 400 Hz each).

The proposed factors are implemented in GTSAM [3], and we used the IMU factor built into GTSAM 4.0 [5] with an incremental solver iSAM2 [2]. We used a semi-direct visual odometry library SVO 2.0 [26] with the Multisense S7 camera. The camera recorded synchronized stereo images at 20 Hz and IMU measurements in about 750 Hz. SVO processes those measurements in real-time and outputs 6

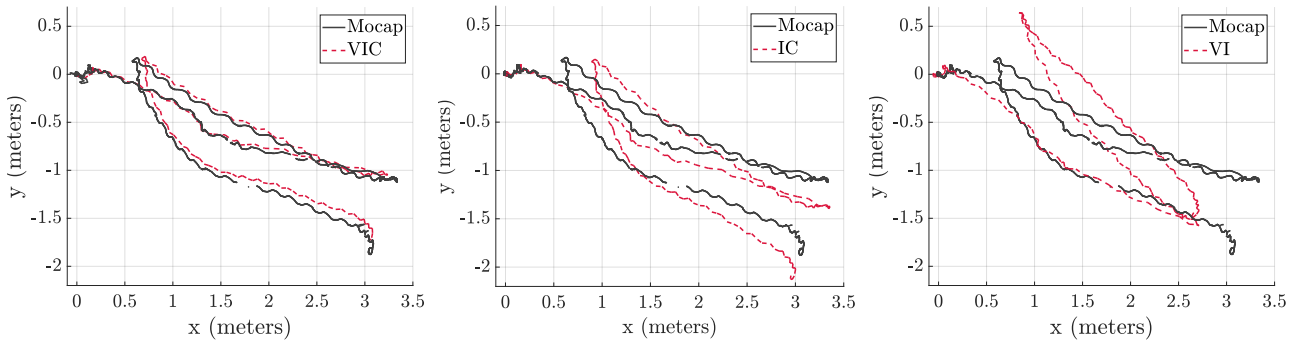


Fig. 5: The odometry results from a 60 second walking experiment using a Cassie-series robot. The Visual-Inertial-Contact (VIC) odometry outperformed both the Inertial-Contact (IC), and the Visual-Inertial (VI) odometry. “Ground-truth” data was collected from a Vicon motion capture system. It is important to note that no loop-closures are being performed, which helps to explain the relatively poor odometry from VI. The video of this experiment is provided at <https://youtu.be/WDPHd15g2MQ>.

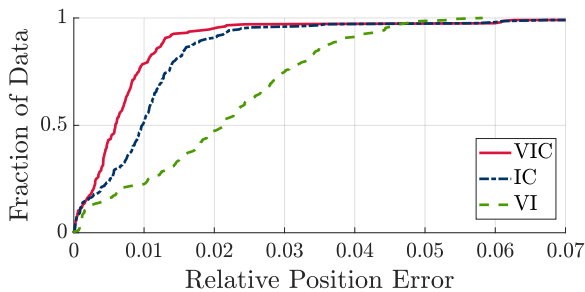


Fig. 6: The Cumulative Distribution Function (CDF) of the relative position error provides a way to analyze the drift in the odometry estimates from various combinations of factors. The fraction of data corresponding to small relative position errors (low-drift odometry) is the larger for Visual-Inertial-Contact (VIC) odometry than for Inertial-Contact (IC) or Visual-Inertial (VI) odometry.

degrees of freedom poses of the left camera in a fixed world frame, \mathbf{X}_i , for the current time-step i . The relative transformation of the camera from time-step i to j can be obtained using $\Delta\mathbf{X}_{ij} = \mathbf{X}_i^{-1}\mathbf{X}_j$. We selected keyframes approximately every 0.25 seconds and added a pose factor for connecting any two corresponding successive keyframes in the graph.

B. First Experiment: Odometry Comparison

In this experiment, we had Cassie stand in place for about 15 seconds, then slowly walk forwards and backwards along the length of the lab for approximately 45 seconds. The resulting data was used to compare the odometry performance (processed off-line) of different combinations of factors. The results are shown in Figure 5. The odometry estimate from VIC, as expected, outperforms all other combinations of factors. The Cumulative Distribution Function (CDF) of the relative position error is shown in Figure 6. The relative position CDF provides a method for analyzing the drift of an odometry estimate.

From Figure 6, it can be seen that VIC has the highest fraction of data corresponding to smaller relative position errors. This means VIC has lowest drift among all odometry

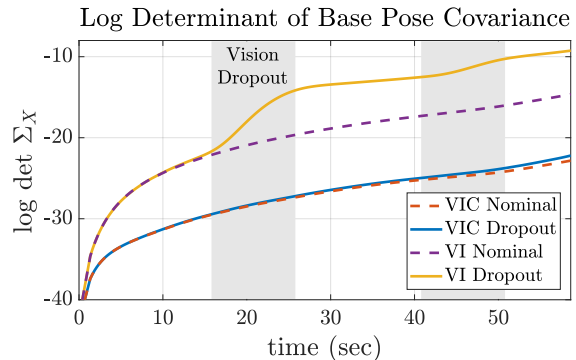


Fig. 7: When vision data is lost, the covariance of the robot’s base pose sharply grows for VI odometry due to the lack of additional measurements to constrain the graph. In contrast, during “vision dropout” periods, the additional contact factors allows the covariance estimate from VIC to remains close to the nominal case.

systems. When the robot is walking, the hard impacts cause significant camera shake which leads to motion blur in the images. This effect, along with possibly the lab environment lacking numerous quality features, helps to explain the relatively poor VI odometry performance.

C. Second Experiment: Vision Dropout

One of the main benefits from including FK and contact factors is that the state estimator can be more robust to failure of the vision system. In this experiment, we simulate the effects of “vision dropout” by simply ignoring SVO visual-odometry data for two 10-second periods of the experimental data described in the previous section. In other words, during a “vision dropout” period, VIC odometry reduces to IC odometry, and VI odometry reduces down to inertial (I) odometry. Figure 7 shows the log determinant of the base pose covariance for VIC and VI for these “vision dropout” experiments. The larger the log determinant, the more uncertain the estimator is about the robot’s base pose. During the “vision dropout” periods, uncertainty grows for VI odometry. This sharp covariance growth is due to the lack of additional sensor measurements to add into the factor

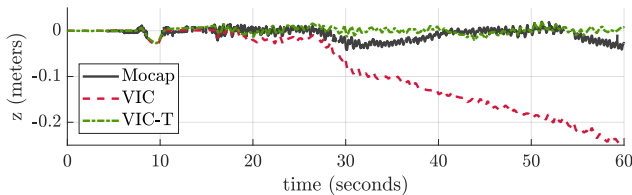


Fig. 8: Since the contact pose is now part of the estimated state, it is possible to add “terrain factors” that relate this contact pose to a prior map. Adding the simple constraint that the contact frame z-translation is zero (VIC-T) improves the drift in the z-direction when compared to the nominal Visual-Inertial-Contact (VIC) case.

graph. In contrast, the covariance growth for VIC is hardly affected over the same dropout periods.

D. Third Experiment: Terrain Factors as Loop-Closures

Another benefit of adding the proposed contact factors comes from the addition of the contact frame poses into the robot’s state. With these new state variables, it becomes simple to place additional constraints that relate the contact pose to a prior map. We test this idea on the collected experiment data by recognizing that the ground was relatively flat in the laboratory. This “zero-height” elevation data serves as our prior map. Figure 8 shows how adding this trivial constraint can reduce position drift in the z-direction. This experiment simply serves to illustrate the potential for “terrain factors”, as the state estimate could be further improved if the robot was actually mapping out the terrain; there was actually a small downward slope in the lab (as shown in the motion capture data).

VII. CONCLUSION

We developed a novel method for preintegrating contact information through an arbitrary number of contact switches using a hybrid preintegrated contact factor. The proposed approach was verified through experimental evaluations using a Cassie-series robot where a motion capture system is used as a proxy for ground truth data. Our results indicate that the fusion of contact information with IMU and vision data provide a reliable odometry system for legged robot. Furthermore, we showed that the developed visual-inertial-contact odometry system is robust to occasional vision system failures.

In the future, we plan to incorporate loop closure constraints into our factor graph framework to further improve state estimation, paving the way for long-term mapping on legged robots. We also plan to further investigate the potential utility of “terrain factors” to allow the robot’s state to be corrected through detected contact with points on an estimated map.

ACKNOWLEDGMENT

The authors thank Agility Robotics for designing the robot, and Yukai Gong for developing the feedback controller. We also thank Dr. Elliott Rouse and Catherine Kinnaird for providing us with the lab space and equipment necessary to collect and analyze the motion capture data. Funding for R. Hartley, M. Ghaffari Jadidi, L. Gan, and J. Huang is given by the Toyota Research Institute (TRI), partly under award number N021515, however this article solely reflects the opinions and conclusions of its authors and not TRI or any other Toyota entity. Funding for J. Grizzle was in part provided by TRI and in part by NSF Award No. 1525006.

REFERENCES

- [1] M. Bloesch, M. Hutter, M. A. Hoepffinger, S. Leutenegger, C. Gehring, C. D. Remy, and R. Siegwart, “State estimation for legged robots—consistent fusion of leg kinematics and IMU,” in *Robotics: Science and Systems*, Berlin, Germany, June 2013. 1
- [2] M. Kaess, H. Johannsson, R. Roberts, V. Ila, J. J. Leonard, and F. Dellaert, “iSAM2: Incremental smoothing and mapping using the Bayes tree,” *The Int. J. Robot. Res.*, vol. 31, no. 2, pp. 216–235, 2012. 1, 6
- [3] F. Dellaert, “Factor graphs and GTSAM: A hands-on introduction,” Georgia Institute of Technology, Tech. Rep., 2012. 1, 6
- [4] L. Carlone, Z. Kira, C. Beall, V. Indelman, and F. Dellaert, “Eliminating conditionally independent sets in factor graphs: A unifying perspective based on smart factors,” in *Proc. IEEE Int. Conf. Robot. Automat.* IEEE, 2014, pp. 4290–4297. 1
- [5] C. Forster, L. Carlone, F. Dellaert, and D. Scaramuzza, “On-manifold preintegration for real-time visual–inertial odometry,” *IEEE Trans. Robot.*, vol. 33, no. 1, pp. 1–21, 2017. 1, 2, 6
- [6] S. Thrun, Y. Liu, D. Koller, A. Y. Ng, Z. Ghahramani, and H. Durrant-Whyte, “Simultaneous localization and mapping with sparse extended information filters,” *The Int. J. Robot. Res.*, vol. 23, no. 7–8, pp. 693–716, 2004. 1
- [7] R. M. Eustice, H. Singh, and J. J. Leonard, “Exactly sparse delayed-state filters for view-based slam,” *IEEE Trans. Robot.*, vol. 22, no. 6, pp. 1100–1114, 2006. 1
- [8] N. Rotella, M. Bloesch, L. Righetti, and S. Schaal, “State estimation for a humanoid robot,” in *Proc. IEEE/RSJ Int. Conf. Intell. Robots Syst.* IEEE, 2014, pp. 952–958. 1
- [9] M. Benallegue and F. Lamiroux, “Estimation and stabilization of humanoid flexibility deformation using only inertial measurement units and contact information,” *Int. J. Humanoid Robot.*, vol. 12, no. 03, p. 1550025, 2015. 1
- [10] J. Eljaik, N. Kuppuswamy, and F. Nori, “Multimodal sensor fusion for foot state estimation in bipedal robots using the extended kalman filter,” in *Proc. IEEE/RSJ Int. Conf. Intell. Robots Syst.* IEEE, 2015, pp. 2698–2704. 1
- [11] S. Kuindersma, R. Deits, M. Fallon, A. Valenzuela, H. Dai, F. Permenter, T. Koolen, P. Marion, and R. Tedrake, “Optimization-based locomotion planning, estimation, and control design for the atlas humanoid robot,” *Auton. Robot.*, vol. 40, no. 3, pp. 429–455, 2016. 1
- [12] P. Fankhauser, M. Bloesch, C. Gehring, M. Hutter, and R. Siegwart, “Robot-centric elevation mapping with uncertainty estimates,” in *International Conference on Climbing and Walking Robots*, 2014, pp. 433–440. 1
- [13] M. A. Bloesch, “State estimation for legged robots—kinematics, inertial sensing, and computer vision,” Ph.D. dissertation, 2017. 1
- [14] M. F. Fallon, M. Antone, N. Roy, and S. Teller, “Drift-free humanoid state estimation fusing kinematic, inertial and lidar sensing,” in *Humanoid Robots (Humanoids), 2014 14th IEEE-RAS International Conference on.* IEEE, 2014, pp. 112–119. 1
- [15] S. Nobili, M. Camurri, V. Barasuol, M. Focchi, D. G. Caldwell, C. Semini, and M. Fallon, “Heterogeneous sensor fusion for accurate state estimation of dynamic legged robots,” in *Robotics: Science and Systems*, 2017. 1
- [16] G. P. Roston and E. P. Krotkov, “Dead reckoning navigation for walking robots,” Carnegie-Mellon University, Pittsburgh, PA, Robotics Institute, Tech. Rep., 1991. 1
- [17] R. Hartley, J. Mangelson, L. Gan, M. Ghaffari Jadidi, J. M. Walls, R. M. Eustice, and J. W. Grizzle, “Legged robot state-estimation through combined forward kinematic and preintegrated contact factors,” in *Proc. IEEE Int. Conf. Robot. Automat.* IEEE, 2018. 1
- [18] R. M. Murray, Z. Li, S. S. Sastry, and S. S. Sastry, *A mathematical introduction to robotic manipulation.* CRC press, 1994. 2, 4
- [19] G. S. Chirikjian, *Stochastic Models, Information Theory, and Lie Groups, Volume 2: Analytic Methods and Modern Applications.* Springer Science & Business Media, 2011. 2
- [20] P.-A. Absil, R. Mahony, and R. Sepulchre, *Optimization algorithms on matrix manifolds.* Princeton University Press, 2009. 2
- [21] T. D. Barfoot and P. T. Furgale, “Associating uncertainty with three-dimensional poses for use in estimation problems,” *IEEE Trans. Robot.*, vol. 30, no. 3, pp. 679–693, 2014. 2
- [22] E. R. Westervelt, J. W. Grizzle, C. Chevallereau, J. H. Choi, and B. Morris, *Feedback control of dynamic bipedal robot locomotion.* CRC press, 2007. 4

- [23] R. Hartley, M. Ghaffari Jadidi, L. Gan, J.-K. Huang, J. W. Grizzle, and R. M. Eustice, "Supplementary material: Hybrid contact preintegration for visual-inertial-contact state estimation within factor graphs," University of Michigan, Tech. Rep., March 2018. [Online]. Available: <https://www.dropbox.com/sh/urik6o4ksxstjfp/AADqCvcweaqcjKsfhpXA3Ptxa?dl=0> 5, 6
- [24] M. Quigley, K. Conley, B. Gerkey, J. Faust, T. Foote, J. Leibs, R. Wheeler, and A. Y. Ng, "ROS: an open-source Robot Operating System," in *ICRA workshop on open source software*, vol. 3, no. 3.2, 2009, p. 5. 6
- [25] E. Olson, "A passive solution to the sensor synchronization problem," in *Proc. IEEE/RSJ Int. Conf. Intell. Robots Syst.*, October 2010. 6
- [26] C. Forster, Z. Zhang, M. Gassner, M. Werlberger, and D. Scaramuzza, "SVO: Semidirect visual odometry for monocular and multicamera systems," *IEEE Trans. Robot.*, vol. 33, no. 2, pp. 249–265, 2017. 6